
Fiberwise dimensionality reduction of topologically complex data with vector bundles*

Luis Scoccola

Department of Mathematics
Northeastern University
Boston, MA

Jose A. Perea

Department of Mathematics and
Khoury College of Computer Sciences
Northeastern University
Boston, MA

Abstract

Datasets with non-trivial large scale topology can be hard to embed in low-dimensional Euclidean space with existing dimensionality reduction algorithms. We propose to model topologically complex datasets using vector bundles, in such a way that the base space accounts for the large scale topology, while the fibers account for the local geometry. This allows one to reduce the dimensionality of the fibers, while preserving the large scale topology. We formalize this point of view, and, as an application, we describe an algorithm which takes as input a dataset together with an initial representation of it in Euclidean space, assumed to recover part of its large scale topology, and outputs a new representation that integrates local representations, obtained through local linear dimensionality reduction, along the initial global representation. We demonstrate this algorithm on examples coming from dynamical systems and chemistry. In these examples, our algorithm is able to learn topologically faithful embeddings of the data in lower target dimension than various well known metric-based dimensionality reduction algorithms.

1 Introduction

Motivation. We take the manifold hypothesis at face value and consider data consisting of a finite sample of a Riemannian manifold. We take the goal of *dimensionality reduction* to be that of learning an embedding of the input data in low dimension, in such a way that the differentiable structure of the underlying manifold is preserved. This is different from *charting*, whose objective we take to be that of producing local parametrizations of the data that, together, cover the entire manifold.

We refer to dimensionality reduction algorithms which aim to preserve metric relationships and do not explicitly incorporate large scale topology in their objective function as *metric-based*. Metric-based algorithms work best when the Riemannian manifold underlying the data can be isometrically embedded in the target dimension. For example, algorithms such as Isomap [53], Local Tangent Space Alignment (LTSA) [59], and Hessian Eigenmaps (HLE) [16] assume that the manifold \mathcal{X} underlying the data is *isometrically developable*, in the sense that \mathcal{X} is a d -dimensional Riemannian manifold for which there exists an embedded d -dimensional manifold $\mathcal{X}' \subseteq \mathbb{R}^d$ and a diffeomorphism $\mathcal{X}' \rightarrow \mathcal{X}$ which is a Riemannian isometry. An isometrically developable manifold \mathcal{X} is necessarily *flat* (i.e., locally isometric to Euclidean space) and *developable* (i.e., diffeomorphic to an embedded d -dimensional manifold $\mathcal{X}' \subseteq \mathbb{R}^d$). But a manifold can be flat and developable without it being isometrically developable: a simple example is that of a straight cylinder in \mathbb{R}^3 (Fig. 1). As observed in [25], and shown in Fig. 1, already in the setting of a flat and developable d -dimensional manifold, metric-based dimensionality reduction algorithms can fail to find an embedding of the data in \mathbb{R}^d .

* This work was partially supported by the National Science Foundation through grants CCF-2006661 and CAREER award DMS-1943758.

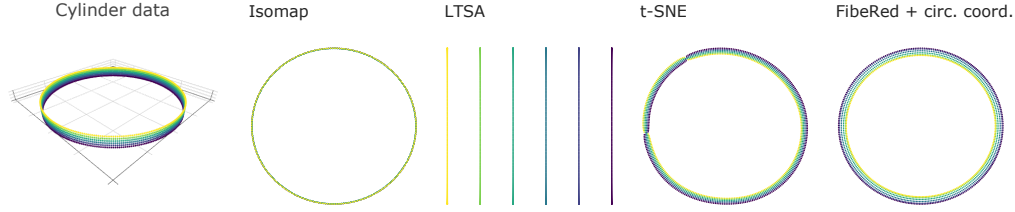


Figure 1: **1:** A sample from a cylinder with height equal to 0.15 times its radius, colored by height. The cylinder is developable, since it is diffeomorphic to an annulus in \mathbb{R}^2 , and is also flat, but it is not isometric to the annulus, which also has a flat, yet distinct, Riemannian metric. **2,3,4:** Well known dimensionality reduction algorithms run on the cylinder data. The outputs are representative of other parameter choices and of the output of Laplacian Eigenmaps (LE) [8], Diffusion Maps (DM) [14], LLE [43], HLLE, t-SNE [55], and UMAP [29]. Some algorithms only capture the circularity (**2**), others only the local 2D structure (**3**), while others (**4**) capture both, but they are not able to consistently align the local 2D structure. **5:** The output of fiberwise dimensionality reduction.

On the mathematical side, while Whitney’s embedding theorem [57] guarantees that any closed d -dimensional manifold admits a smooth (C^∞) embedding in $2d$ dimensions, a smooth, Riemannian isometric embedding of a closed d -dimensional Riemannian manifold can require in the order of d^2 dimensions [11]. Thus, the preservation of distances requires more complicated embeddings than the preservation of topology.

If we remove a small portion of the cylinder of Fig. 1, in order to make it a curved rectangle, most metric-based dimensionality reduction algorithms have no problem finding an embedding in \mathbb{R}^2 . It is thus the non-trivial topology of the cylinder—its circularity—that causes difficulties. This suggests that embeddings of topologically non-trivial manifolds can be built by gluing local representations along a representation of the global topological structure: in the case of the cylinder, one would try to glue 2D patches around a circle in a globally consistent manner. This leads to the following problem, formalized as the vector bundle embedding problem (Problem 1):

Given a dataset X and an initial map $X \rightarrow \mathbb{R}^D$ capturing the large scale topology of X , find a new representation $X \rightarrow \mathbb{R}^D$ that captures the large scale topology as well as the local geometry.

We call our approach to the above problem *fiberwise dimensionality reduction* (FIBERED). In the examples of Section 5, we focus on manifolds with an essential loop, and, as initial map, we use circular coordinates based on persistent cohomology [15, 38], a technique from Topological Data Analysis [33, 18]. Nevertheless, FIBERED is not restricted to the case of a circular initial embedding.

Contributions. We show that the theory of vector bundles is useful in abstracting (Section 3.1), devising solutions to (Section 4), and computing obstructions to solving (Section 3.3) the problem of extending an initial coarse representation of data to a new, more descriptive representation. We demonstrate with computational examples (Section 5) that efficient embeddings and chartings of topologically non-trivial data can be learned with this approach, and give examples supporting the claim that metric-based dimensionality reduction algorithms are often not able to find such representations. Our main algorithm, FIBERED, can be efficiently implemented; an implementation can be found at [46].

Related work. Various dimensionality reduction schemes [52, 42, 10] learn a global alignment of local linear models from the local interactions of the models, which can be challenging in the presence of non-trivial topology. In contrast, our approach assumes a global topological representation is given, and builds and aligns the local linear models along this representation.

There has been recent interest in designing topology-preserving dimensionality reduction schemes [27, 58, 32, 56]. Our approach is different from previous approaches we are aware of, as it builds a new representation around an initial topological representation, instead of using topology to regularize an essentially metric objective.

The cut-unfold technique of Section 4.7 has a similar goal to that of [25, 58], which propose to tear a data manifold in order to find efficient representations of it. A main difference is that our technique allows the user to select a specific hole to cut, and to use topological persistence to guide this choice.

2 Background and notation

We give a brief description of the main topological notions relevant to this paper. We include detailed references for the interested reader.

Vector bundles. We assume that manifolds, vector bundles, maps, and metrics are all smooth, i.e., C^∞ . For an introduction, we refer the reader to, e.g., [31, 23].

A *cover* of a topological space \mathcal{B} is an indexed collection $\mathcal{U} = \{U_i\}_{i \in I}$ of open sets of \mathcal{B} such that $\mathcal{B} = \bigcup_{i \in I} U_i$. When there is no risk of confusion, we may omit the indexing set.

A rank r (smooth) *vector bundle* $\pi : \mathcal{X} \rightarrow \mathcal{B}$ consists of a smooth map of differentiable manifolds such that each fiber $\pi^{-1}(b) \subseteq \mathcal{X}$ is endowed with the structure of a dimension r real vector space, and such that there exists a cover $\mathcal{U} = \{U_i\}$ of \mathcal{B} and diffeomorphisms $(\pi|_{\pi^{-1}(U_i)}, f_i) : \pi^{-1}(U_i) \rightarrow U_i \times \mathbb{R}^r$ that induce a linear isomorphism $f_i|_{\pi^{-1}(b)} : \pi^{-1}(b) \rightarrow \mathbb{R}^r$ for each $b \in U_i \subseteq \mathcal{B}$. The spaces \mathcal{X} and \mathcal{B} are called the *total space* and the *base space*, respectively, and the maps $\{(\pi|_{\pi^{-1}(U_i)}, f_i) : \pi^{-1}(U_i) \rightarrow U_i \times \mathbb{R}^r\}$ are called a *trivialization* of the vector bundle π .

A vector bundle $\pi : \mathcal{X} \rightarrow \mathcal{B}$ is *Euclidean* if each of its fibers $\pi^{-1}(b)$ is endowed with a scalar product $\langle -, - \rangle_b$ that varies smoothly with $b \in \mathcal{B}$. A *metric trivialization* of a Euclidean vector bundle $\pi : \mathcal{X} \rightarrow \mathcal{B}$ consists of a trivialization in which the induced linear isomorphisms $\pi^{-1}(b) \rightarrow \mathbb{R}^r$ are isometries, where \mathbb{R}^r is endowed with its usual scalar product.

A *Riemannian manifold* consists of a smooth manifold \mathcal{B} together with a Euclidean vector bundle structure on its tangent vector bundle $T\mathcal{B} \rightarrow \mathcal{B}$.

Let $n \leq m$. The (compact) *Stiefel manifold* $V(n, m)$ consists of the space of m -by- n matrices with orthonormal columns, endowed with its usual differentiable structure. When $n = m$, the Stiefel manifold $V(n, n)$ is equal to the *orthogonal group* $O(n)$ of orthogonal n -by- n matrices.

A *partition of unity* subordinate to a cover $\mathcal{U} = \{U_i\}$ of a topological space \mathcal{B} consists of a family of continuous functions $\{\rho_i : \mathcal{B} \rightarrow \mathbb{R}\}$ taking non-negative values such that $\rho_i(x) = 0$ if $x \notin U_i$, for all $x \in \mathcal{B}$ we have that $\rho_i(x) \neq 0$ for only finitely many $i \in I$, and such that $\sum_i \rho_i(x) = 1$ for all $x \in \mathcal{B}$.

Simplicial complexes. A *simplicial complex* consists of a set S together with a family $\text{simp}(S)$ of non-empty, finite subsets S , called *simplices*, that is closed under taking subsets and that contains all singletons. Any graph G gives rise to a simplicial complex whose underlying set is the set of vertices of G , and whose simplices consist of the vertices and the edges of G . Another important example is that of the *nerve* of a cover $\mathcal{U} = \{U_i\}_{i \in I}$ of a topological space. The underlying set of the nerve of \mathcal{U} is I , while the simplices consist of all finite subsets $J \subseteq I$ such that $\bigcap_{j \in J} U_j \neq \emptyset$.

(Persistent) cohomology. We briefly recall some of the properties of cohomology [21] and persistence [18]. Given a topological space \mathcal{B} , a field \mathbb{k} , and $n \in \mathbb{N}$, the *n th cohomology group* of \mathcal{B} with coefficients in \mathbb{k} is a \mathbb{k} -vector space $H^n(\mathcal{B}; \mathbb{k})$, whose dimension, informally, counts the number of n -dimensional wholes in \mathcal{B} . Cohomology is a functorial operation, which in particular implies that, given a family of topological spaces $\{\mathcal{B}_s\}_{s \in \mathbb{R}}$ such that $\mathcal{B}_s \subseteq \mathcal{B}_{s'}$ for $s \leq s'$, there exist linear maps $(s \leq s')^* : H^n(\mathcal{B}_{s'}; \mathbb{k}) \rightarrow H^n(\mathcal{B}_s; \mathbb{k})$ such that $(s \leq s')^* \circ (s' \leq s'')^* = (s \leq s'')^*$ for all $s \leq s' \leq s'' \in \mathbb{R}$.

Under mild hypothesis, the family of \mathbb{k} -vector spaces and linear maps $\{H^n(\mathcal{B}_{s'}; \mathbb{k}) \rightarrow H^n(\mathcal{B}_s; \mathbb{k})\}$ can be described by a *persistence diagram* (PD) [33, Chapter 1, Section 3], which consists of a finite multiset of points $\{(x_i, y_i) \in \mathbb{R}^2 : y_i > x_i\}$, which has the property that the rank of the linear map $H^n(\mathcal{B}_{s'}; \mathbb{k}) \rightarrow H^n(\mathcal{B}_s; \mathbb{k})$ is equal to the number of points (x_i, y_i) such that $x_i \leq s \leq s' < y_i$. Informally, a point (x_i, y_i) in the n th persistence diagram of a filtered topological space $\{\mathcal{B}_s\}_{s \in \mathbb{R}}$ represents a hole in the filtration that first appears in \mathcal{B}_{x_i} and disappears (is filled) in \mathcal{B}_{y_i} .

When $\{\mathcal{B}_s\}$ is a well-behaved filtration, such a filtration of a finite simplicial complex, persistent cohomology can be used to construct cohomological coordinates, which are maps from the space that is being filtered into a topologically interesting space [15, 38, 36, 39]. We use *circular coordinates* as in [38], which, given a choice of point in the persistence diagram of the first cohomology group of the Vietoris–Rips filtration [18, Definition 1.2] of (a subsample of) the data, returns a map from the data into the circle. The main takeaway here is that circular coordinates give a map into the circle which captures circularity present in the data.

3 Theory

3.1 The vector bundle embedding problem

For background, please refer to Section 2 and the references therein. In Section 3.3 we explain how characteristic classes of vector bundles give computable obstructions to solving the vector bundle embedding problem, and can thus be used for parameter selection.

Let \mathcal{B} be a closed differentiable manifold and let $\pi : \mathcal{X} \rightarrow \mathcal{B}$ be a rank r Euclidean vector bundle with zero-section $s_0 : \mathcal{B} \rightarrow \mathcal{X}$, where by *Euclidean* we mean that π is endowed with a scalar product on each fiber $\pi^{-1}(b) \subseteq \mathcal{X}$, which varies smoothly with $b \in \mathcal{B}$. The main problem we seek to solve is that of extending an embedding $\iota : \mathcal{B} \rightarrow \mathbb{R}^D$ to a fiberwise isometric embedding of \mathcal{X} , as follows:

Problem 1. *Given an embedding $\iota : \mathcal{B} \rightarrow \mathbb{R}^D$, find a fiberwise isometric embedding $\bar{\iota} : \mathcal{X} \rightarrow \mathbb{R}^D$ that extends ι in the sense that $\bar{\iota} \circ s_0 = \iota$, and that is orthogonal to \mathcal{B} , in the sense that $\bar{\iota}(\pi^{-1}(b)) \perp \iota(T_b \mathcal{B})$ for all $b \in \mathcal{B}$.*

By *fiberwise isometric embedding* $\mathcal{X} \rightarrow \mathbb{R}^D$ we mean a map that is a linear isometry when restricted to each fiber $\pi^{-1}(b) \subseteq \mathcal{X}$, where $b \in \mathcal{B}$.

Let $\nu : N \rightarrow \mathcal{B}$ be the normal bundle of the embedding $\iota : \mathcal{B} \rightarrow \mathbb{R}^D$, and endow ν with the Euclidean structure inherited from \mathbb{R}^D . The following result reduces Problem 1 to a problem only involving vector bundles.

Lemma 2. *Problem 1 admits a solution if and only if there exists a morphism $\mathcal{X} \rightarrow N$ of vector bundles over \mathcal{B} that is injective and an isometry in each fiber.*

As is usual when working with bundles, one can solve Problem 1 locally. In order to do this, we trivialize the bundles \mathcal{X} and N over a common cover of the base \mathcal{B} , and construct the embedding $\mathcal{X} \rightarrow N$ by restricting to each element of the cover. Formally, we proceed as follows.

Let e be the dimension of \mathcal{B} , so that the rank of ν is $D - e$. Let $\mathcal{U} = \{U_i\}$ be a cover of \mathcal{B} such that both π and ν can be trivialized over \mathcal{U} , and let $\mathcal{X}_i := \pi^{-1}(U_i)$. Recall that $V(n, m)$ denotes the Stiefel manifold, which consist of m -by- n matrices with orthonormal columns, and that $O(n) = V(n, n)$ denotes the orthogonal group. Let $\alpha = \{\alpha_i : U_i \rightarrow V(D - e, D)\}$ be local bases for N , and let $\Theta = \{\Theta_{ij} : U_i \cap U_j \rightarrow O(D - e)\}$ be defined by $\Theta_{ij}(b) = \alpha_i(b) \circ \alpha_j(b)^T$ for all $b \in U_i \cap U_j$, so that Θ is a cocycle with associated vector bundle ν . Finally, let $\{(\pi|_{\mathcal{X}_i}, f_i) : \mathcal{X}_i \rightarrow U_i \times \mathbb{R}^r\}$ be a metric trivialization of \mathcal{X} over \mathcal{U} , and let $\Omega = \{\Omega_{ij} : U_i \cap U_j \rightarrow O(r)\}$ be defined as the unique set of maps satisfying

$$\Omega_{ij}(\pi(x)) f_j(x) = f_i(x), \text{ for all } x \in \mathcal{X}_i \cap \mathcal{X}_j, \quad (1)$$

so that Ω is a cocycle with associated vector bundle π . We refer to the maps $\{f_i : \mathcal{X}_i \rightarrow \mathbb{R}^r\}$ as the *fiber coordinates*. With these definitions, one can use Lemma 2 to prove the following.

Proposition 3. *There exists a fiberwise isometric embedding $\mathcal{X} \rightarrow N$ if and only if there exist maps $\Phi = \{\Phi_i : U_i \rightarrow V(r, D - e)\}$ such that*

$$\Phi_i(b) \Omega_{ij}(b) = \Theta_{ij}(b) \Phi_j(b), \text{ for all } i \text{ and } j \text{ and } b \in U_i \cap U_j. \quad (2)$$

Given the maps $\Phi = \{\Phi_i : U_i \rightarrow V(r, D - e)\}$ of Proposition 3, one obtains the fiberwise isometric embedding $\bar{\iota} : \mathcal{X} \rightarrow \mathbb{R}^D$ by $\bar{\iota}(x) = \alpha_i(b) \Phi_i(b) f_i(x) + \iota(b)$, where $b = \pi(x)$.

In general, the fiberwise isometric embedding $\bar{\iota} : \mathcal{X} \rightarrow \mathbb{R}^D$ is not an embedding of \mathcal{X} as a manifold, since different fibers may intersect. Nonetheless, if $\tau > 0$ is the *reach* ([1, Definition 2.1]) of $\iota(\mathcal{B}) \subseteq \mathbb{R}^D$, i.e., the largest possible radius of a uniform tubular neighborhood around $\iota(\mathcal{B})$, one can find an embedding of a full-dimensional compact subset of \mathcal{X} by scaling the fibers by a fraction of τ , as follows. Let $\text{disk}(\pi) \subseteq \mathcal{X}$ be the unit disk of the bundle π , namely, the subspace of points $x \in \mathcal{X}$ such that $\|x - s_0(\pi(x))\| \leq 1$, where $\|\cdot\|$ denotes the norm of the fiber $\pi^{-1}(\pi(x))$ induced by the Euclidean structure of π . Then, the following formula gives an embedding $\text{disk}(\pi) \rightarrow \mathbb{R}^D$:

$$x \mapsto c\tau \cdot \alpha_i(\pi(x)) \Phi_i(\pi(x)) f_i(x) + \iota(\pi(x)), \text{ for } \pi(x) \in U_i, \quad (3)$$

where $0 < c < 1$ is any fixed constant.

3.2 Vector bundles from finite samples

In practice, continuous maps to a Stiefel manifold or orthogonal group—such as the maps $\{\alpha_i : U_i \rightarrow \mathcal{V}(D - e, D)\}$ or the cocycle $\{\Omega_{ij} : U_i \cap U_j \rightarrow O(r)\}$ of Section 3.1—are hard to work with, as they are potentially determined by an infinite amount of data. One of the main takeaways of [45] is that one can work with Euclidean vector bundles in practice by considering only constant maps into Stiefel manifolds or orthogonal groups. In order to accomplish this, one relaxes the notion of Euclidean vector bundle as follows.

Given a simplicial complex S , a rank r *discrete approximate* cocycle on S ([45, Definition 5.1]) consists of a family of matrices $\{\Omega_{ij} \in O(r)\}$ indexed by the oriented 1-simplices of S which satisfies $\Omega_{ij} = \Omega_{ji}^T$. There is a similar way of discretizing maps into a Stiefel manifold ([45, Definition 5.4]). These discretizations can be used to represent usual vector bundles [45, Theorem A] and any vector bundle can be represented in this way [45, Proposition 5.7].

This justifies the fact that, in Section 4, we discretize the base \mathcal{B} by considering the simplicial complex given by the nerve of a cover $\mathcal{U} = \{U_i\}$, and we consider constant maps from U_i into a Stiefel manifold and from $U_i \cap U_j$ into an orthogonal group.

3.3 Computable obstructions to vector bundle embedding

The theory of vector bundles provides us with algebraic obstructions to solving Problem 1, namely, characteristic classes. We now give a few details about the subject; we refer the reader to [31] for a detailed account of the theory of characteristic classes.

To a vector bundle $\pi : \mathcal{X} \rightarrow \mathcal{B}$ and number $i \in \mathbb{N}$, one can associate an element $w_i(\pi) \in H^i(\mathcal{B}; \mathbb{Z}/2)$ of the i th cohomology group of \mathcal{B} with coefficients in the two-element group $\mathbb{Z}/2$, called the *ith Stiefel–Whitney class* of π . This procedure is such that, if π and π' are isomorphic vector bundles over the same base \mathcal{B} , then $w_i(\pi) = w_i(\pi')$.

To give some intuition, we mention the well known fact that the first Stiefel–Whitney class of a vector bundle is zero if and only if the vector bundle is orientable, in the sense that one can orient all fibers in such a way that the orientation is preserved by some trivialization.

If Problem 1 admits a solution, then there exists a complement of π in ν , that is there exists a rank $D - b - r$ vector bundle κ over \mathcal{B} such that $\pi \oplus \kappa \cong \nu$, where \oplus denotes the direct sum of vector bundles. It follows from the Whitney product formula [31, Section 4, Axiom 3] that $w(\pi) \smile w(\kappa) = w(\nu)$, where \smile denotes the cup-product in cohomology [21, Section 3.2]. In particular, when Problem 1 admits a solution, we have the following:

- If $D = r + e$, then $w_1(\pi) = w_1(\nu) \in H^1(\mathcal{B}; \mathbb{Z}/2)$.
- If $D = r + e + 1$, then $w_2(\pi) - w_1(\pi)^2 + w_1(\pi) \smile w_1(\nu) = w_2(\nu) \in H^2(\mathcal{B}; \mathbb{Z}/2)$.

These equalities are obstructions to the existence of a solution to Problem 1: indeed, if any of these equalities is not satisfied, then Problem 1 does not admit a solution. Using the algorithms of [45, Theorem C], these obstructions can be effectively computed from finite samples.

In Appendix B.3 we show the result of computing these obstructions for the examples of Section 5, which we use to select the target dimension D .

4 The fiberwise dimensionality reduction scheme

We describe the FIBERED algorithm in Sections 4.2 and 4.3. In Section 4.7, we explain how we choose parameters. Since we work with finite samples, we need to use a discrete representation of vector bundles; for this we use discrete approximate cocycles, as in [45] (see Section 3.2 for details).

To facilitate the interpretation of the different steps of the algorithm, the notation is kept as in Section 3.1, except for the spaces \mathcal{X} and \mathcal{B} , which we denote here by X and B to emphasize the fact that we are working with finite samples $X \subseteq \mathcal{X}$ and $B \subseteq \mathcal{B}$. Precise assumptions about the input of the algorithm are in Section 4.1. We remark that our algorithm can be efficiently implemented; we give more details in Appendix B.1.

4.1 Assumptions about input of FIBERED

The assumptions here are made so that we can justify the steps of the algorithm; formally addressing the consistency of the algorithm is left for future work.

We assume that there exists a closed manifold \mathcal{B} of dimension e , a rank r Euclidean vector bundle $\pi : \mathcal{X} \rightarrow \mathcal{B}$, a Riemannian metric on \mathcal{X} , and a smooth embedding $\iota : \mathcal{B} \rightarrow \mathbb{R}^D$. We assume that the Riemannian metric on \mathcal{X} is compatible with the Euclidean structure of the vector bundle π , in the sense that, given any metric trivialization of π by maps $\{(\pi|_{\mathcal{X}_i}, f_i) : \mathcal{X}_i \rightarrow U_i \times \mathbb{R}^r\}$, and $x \in \mathcal{X}$, the composite

$$\mathbb{R}^r \rightarrow T_{\pi(x)}\mathcal{B} \oplus T_{f_i(x)}\mathbb{R}^r \xrightarrow{(d(\pi|_{\mathcal{X}_i}, f_i)_x)^{-1}} T_x\mathcal{X}$$

is a linear isometric monomorphism. Here, the first map is the inclusion in the second component of the direct sum, where we are using the standard identification between tangent spaces of a Euclidean space and the Euclidean space itself.

The input metric space of FIBERED is assumed to be a sample $X \subseteq \mathcal{X}$, which implies, in particular, that its image $B := \pi(X)$ is a sample $B \subseteq \mathcal{B}$.

Note that we do not ask for the embedding $\iota : \mathcal{B} \rightarrow \mathbb{R}^D$ to preserve the Riemannian structure of \mathcal{B} inherited from that of \mathcal{X} . Note also that, when solving the vector bundle embedding problem, only the Euclidean structure of π is required to be preserved, although we assumed that the total space \mathcal{X} has a (compatible) Riemannian metric. We require a metric on \mathcal{X} since most datasets come with a (global) distance, so we need to make some assumption about how this distance is generated.

4.2 Main routine

Inputs. A dataset represented by a finite set X together with a distance matrix $\partial : X \times X \rightarrow \mathbb{R}$; and a function $\pi : X \rightarrow \mathbb{R}^D$. We let $B := \pi(X) \subseteq \mathbb{R}^D$.

Parameters. A number $k \in \mathbb{N}$, the number of sets we use to construct a cover of B ; a number $\text{n_iter} \in \mathbb{N}$ used in the ALIGNFIBERS subroutine; an estimate $e \in \mathbb{N}$ of the intrinsic dimension of \mathcal{B} ; an estimate $d \in \mathbb{N}$ of the intrinsic dimension of \mathcal{X} ; a fiber scale $0 < c < 1$.

Output. A new map $X \rightarrow \mathbb{R}^D$.

Algorithm 1 FIBERED($X, \pi, k, e, d, c, \text{n_iter}$)

```

1:  $\mathcal{U}, \rho \leftarrow \text{COVERANDPARTITIONUNITY}(k, B)$ 
2:  $\mathcal{N} \leftarrow \text{NERVE}(B, \mathcal{U})$ 
3: for  $1 \leq i \leq k$  do
4:    $\ell_i \leftarrow \text{LOCALLINEARREPRESENTATION}(X, \mathcal{U}, d, i)$ 
5:    $\Psi_i, \alpha_i \leftarrow \text{ESTTANGANDNORMBUN}(B, \mathcal{U}, e, i)$ 
6:    $\bar{f}_i \leftarrow \text{ESTNORMFIBERCOORDINATES}(B, \Psi_i, \ell_i)$ 
7: end for
8:  $\tau \leftarrow \text{ESTREACH}(B, \mathcal{U}, \Psi)$ 
9: for  $(ij) \in \mathcal{N}$  do
10:   $\Omega_{ij}, \Theta_{ij} \leftarrow \text{ESTCOCYCLES}(\bar{f}_i, \bar{f}_j, \alpha_i, \alpha_j)$ 
11: end for
12:  $\Phi \leftarrow \text{ALIGNFIBERS}(\mathcal{N}, \Omega, \Theta, \text{n\_iter})$ 
13: return  $\text{ASSEMBLE}(\rho, \tau, c, \alpha, \Phi, \bar{f}, \pi)$ 

```

4.3 Subroutines

Compute cover and partition of unity (COVERANDPARTITIONUNITY). We compute a cover $\mathcal{U} = \{U_i \subseteq B\}_{1 \leq i \leq k}$ of B as follows. We first run on B an approximate algorithm for the k -center problem. We use a simple, greedy approach, but more sophisticated options are available (see, e.g., [17] for a survey). This results in k points $\{b_1, \dots, b_k\} \subseteq B$ and in a radius $c > 0$ such that any point of B is at distance at most c from some b_i . We then let $U_i = \{b \in B : \|b - b_i\| < 3c\}$. The factor of 3 is arbitrary; we choose it to ensure that elements of the cover have sufficiently large intersections.

We compute a partition of unity $\rho = \{\rho_i : U_i \rightarrow \mathbb{R}\}$ subordinate to \mathcal{U} by first defining $p_i(x) = \exp(-1/(1 - (\|x - b_i\|/(3c))^2))$ for $x \in U_i$ and $p_i(x) = 0$ for $x \notin U_i$, and then normalizing as follows $\rho_i(x) = p_i(x) / \sum_j p_j(x)$.

Compute nerve of cover (NERVE). We let \mathcal{N} be the undirected graph with vertices $1 \leq i \leq k$ and an edge (ij) with weight $s_{ij} = |U_i \cap U_j|$ when $U_i \cap U_j \neq \emptyset$.

Compute local linear representation (LOCALLINEARREPRESENTATION). Given $1 \leq i \leq k$, we let $X_i := \pi^{-1}(U_i)$ and apply a linear dimensionality reduction algorithm to each X_i , resulting in a

function $\ell'_i : X_i \rightarrow \mathbb{R}^d$. In our implementation, we use classical multidimensional scaling (see, e.g., [9]). We then mean-center ℓ'_i to get a function $\ell_i : X_i \rightarrow \mathbb{R}^d$.

Estimate local trivialization of tangent and normal bundle (ESTTANGANDNORMBUN). Given $1 \leq i \leq k$, we compute an orthonormal frame $\Psi_i \in V(e, D)$ by applying PCA with target dimension e to $U_i \subseteq \mathbb{R}^D$. We then compute an orthonormal frame $\alpha_i \in V(D - e, D)$ such that $\alpha_i \perp \Psi_i$.

Estimate normalized fiber coordinates (ESTNORMFIBERCOORDINATES). Given $1 \leq i \leq k$, we define $t : X_i \rightarrow \mathbb{R}^e$ by $t(x) = \Psi_i^T(\pi(x) - b_i)$. We find a linear transformation $m : \mathbb{R}^d \rightarrow \mathbb{R}^e$, which has minimal Frobenius norm and minimizes

$$\sum_{x \in X_i} \|t(x) - m(\ell_i(x))\|^2, \quad (4)$$

and compute an orthonormal frame $\eta_i \in V(r, d)$ with image in the kernel of m . We let $f_i := \eta_i^T \circ \ell_i : X_i \rightarrow \mathbb{R}^r$, and obtain a normalized fiber coordinate $\bar{f}_i : X_i \rightarrow \mathbb{R}^r$ with image contained in the unit ball by normalizing f_i . We justify these choices in Section 4.6.

Estimate reach (ESTREACH). If $\{b_1, \dots, b_k\} \subseteq B$ are the centers of the k balls used to construct the cover \mathcal{U} in COVERANDPARTITIONUNITY, we compute an estimate of the reach of B by

$$\tau = \inf_{i \neq j} \frac{\|b_j - b_i\|^2}{2\sqrt{\|b_j - b_i\|^2 - \|\Psi_i^T(b_j - b_i)\|^2}}.$$

This formula is equivalent to [1, Equation 6.1], where it is proven that, under suitable assumption, it yields a consistent estimator of the reach.

Estimate cocycles for ν and π (ESTCOCYCLES). Based on Eq. (1), given $(ij) \in \mathcal{N}$, we compute an orthogonal matrix $\Omega_{ij} \in O(r)$ which minimizes

$$\sum_{x \in X_i \cap X_j} \|\Omega_{ij} f_j(x) - f_i(x)\|^2.$$

We also compute an orthogonal matrix $\Theta_{ij} \in O(D - e)$ which minimizes $\|\Theta_{ij} - \alpha_i^T \alpha_j\|_F$, where $\|\cdot\|_F$ denotes the Frobenius norm. Both minimizations are instances of the orthogonal Procrustes problem, which can be solved using SVD (see, e.g., [22, Section 7.4]).

Align fibers (ALIGNFIBERS). Based on Eq. (2), we compute orthonormal frames $\{\Phi_i \in V(r, D - e)\}$ minimizing the following expression; we describe the minimization procedure in Section 4.4.

$$\sum_{(ij) \in \mathcal{N}} s_{ij} \|\Phi_i \Omega_{ij} - \Theta_{ij} \Phi_j\|_F. \quad (5)$$

Compute final representation (ASSEMBLE). Based on Eq. (3), we represent $x \in X$ by

$$\sum_{1 \leq i \leq k} \rho_i(x) (c\tau \cdot \alpha_i \Phi_i \bar{f}_i(x) + \pi(x)).$$

4.4 Minimizing Eq. (5)

The minimization problem in ALIGNFIBERS is non-convex, so a possible solution is to do gradient descent in a product Stiefel manifold. This is the approach we take, except that we avoid explicitly computing a gradient, and take a sampling based approach, as done in, e.g., LargeVis [51]. Before describing the approach, we note that, in the case $D = r + e$, the Stiefel manifold $V(r, r)$ is equal to the orthogonal group $O(r)$, which is disconnected. Thus, in this case, any local optimization approach to minimizing Eq. (5), such as gradient descent, is bound to fail. In Section 4.5 we describe a procedure based on the notion of synchronization (see, e.g., [48]), which reduces the problem from having to align using matrices in $O(r)$ to using matrices in $SO(r)$, which is connected.

Iterative procedure. We start by initializing $\{\Phi_i \in V(r, D - e)\}$ at random and setting $a = 1$. For $1 \leq n \leq \text{n_iter}$, we proceed as follows. We sample an edge $(ij) \in \mathcal{N}$ with probability proportional to its weight s_{ij} , let M be an orthonormal frame minimizing $\|M\Omega_{ij} - \Theta_{ij}\Phi_j\|_F$, and replace Φ_i with a closest orthonormal frame to the convex combination of matrices $(1 - a)\Phi_i + aM$. Finally, we replace a with $1 - n/\text{n_iter}$.

4.5 Preprocessing in the case $D = r + e$.

In this case, the matrices Φ , Ω , and Θ are in $O(r)$. The preprocessing consists of replacing the matrices $\{\Theta_{ij}\}$ by matrices that induce an equivalent problem to the one of minimizing Eq. (5), but for which the matrices $\{\Phi_i\}$ we look for can be taken to be in the special orthogonal group $SO(r)$, which is connected.

Note that, if we want $\Phi_i \Omega_{ij}$ and $\Theta_{ij} \Phi_j$ to belong to the same connected component of $O(r)$, then we must have $\det(\Omega_{ij}) \det(\Theta_{ij}) = \det(\Phi_i) \det(\Phi_j) \in O(1) = \{-1, +1\}$. This suggests that we can let $\omega_{ij} = \det(\Omega_{ij}) \det(\Theta_{ij}) \in O(1)$ and consider first the problem of finding $\{\lambda_i \in O(1)\}$ such that $\lambda_i \lambda_j = \omega_{ij}$, which leads to minimizing the objective function

$$\sum_{(ij) \in \mathcal{N}} s_{ij} |\omega_{ij} - \lambda_i \lambda_j|^2.$$

This is a well known synchronization problem, for which an approximate solution can be found effectively and efficiently with spectral methods [49, 4]. Here, we use [4, Algorithm 2.3], with $d = 1$, which yields an approximate solution $\{\lambda_i \in O(1)\}$.

Given $\lambda \in O(1) = \{-1, +1\}$ let $M(\lambda) \in O(r)$ be the diagonal matrix with all diagonal entries equal to 1, except for the first one, which is equal to λ . With this in mind, we can replace Θ_{ij} by $M(\lambda_i) \Theta_{ij} M(\lambda_j)$. Having done this, we can now restrict the matrices $\{\Phi_i\}$ to belong to the connected component of $O(r)$ of orthogonal matrices with $+1$ as determinant. More specifically, we now can carry out the optimization procedure described in Section 4.4, but restricting the matrices $\{\Phi_i\}$ to be in $SO(r) \subseteq O(r) = V(r, r)$.

4.6 Justification of estimate of fiber coordinates

Let $x := s_0(b_i) \in \mathcal{X}$. We interpret the local model $\ell_i : X_i \rightarrow \mathbb{R}^d$ as a projection $\ell_i : X_i \rightarrow T_x \mathcal{X} \cong \mathbb{R}^d$ of X_i onto the tangent space at the origin of the fiber $\pi^{-1}(b_i)$. In the idealized case (Section 4.1), the fiber coordinate $f_i : \mathcal{X}_i \rightarrow \mathbb{R}^r$ is given by any map fitting into a fiberwise isometric diffeomorphism $(\pi|_{\mathcal{X}_i}, f_i) : \mathcal{X}_i \rightarrow U_i \times \mathbb{R}^r$. When dealing with finite samples, we approximate f_i by the composite

$$X_i \xrightarrow{\ell_i} T_x \mathcal{X} \xrightarrow{(df_i)_x} T_{f_i(x)} \mathbb{R}^r \cong \mathbb{R}^r.$$

Note that, by assumption, $(df_i)_x$ is the second component of an isometric isomorphism of Euclidean vector spaces $d(\pi, f_i)_x : T_x \mathcal{X} \rightarrow T_{b_i} \mathcal{B} \oplus \mathbb{R}^r$, in which the two direct summands are orthogonal. It is thus sufficient to estimate the first component $d\pi_x : T_x \mathcal{X} \rightarrow T_{b_i} \mathcal{B}$ and to then compose ℓ_i with the orthogonal projection onto the orthogonal complement of $d\pi_x$. We do have an estimate for the composite

$$X_i \xrightarrow{\ell_i} T_x \mathcal{X} \xrightarrow{d\pi_x} T_{b_i} \mathcal{B} \cong \mathbb{R}^e,$$

namely $t = \Psi_i^T \circ \pi|_{X_i} : X_i \rightarrow \mathbb{R}^e$, but, since the embedding $\mathcal{B} \subseteq \mathbb{R}^D$ is not required to preserve the Riemannian structure of \mathcal{B} inherited from that of \mathcal{X} , the map t is an approximation of $d\pi_x \circ \ell_i$ up to a linear map $m : \mathbb{R}^d \rightarrow \mathbb{R}^e$. This justifies finding m by minimizing Eq. (4), and getting the approximate fiber coordinate f_i by composing ℓ_i with the orthogonal projection onto the kernel of m .

4.7 Choosing input and parameters

Parameters. An estimate of the dimensions e of \mathcal{B} and d of \mathcal{X} can be obtained by applying the elbow method to the explained variance of PCA applied to each of the sets U_i and X_i , but more sophisticated algorithms are available; see, e.g., [26]. The parameter k is chosen to be large enough so that the cover \mathcal{U} captures the topology of the base space \mathcal{B} , and such that each open ball of the cover is sufficiently small so that it can be approximated reasonable well by a linear space. In our case, when the base space is the circle, we use $k = 16$. The algorithm is robust to the choice of parameter `n_iter`, which we choose to be 1000 in all of our examples.

Choosing base map and D . In the examples, we construct the initial map $\pi : X \rightarrow \mathbb{R}^D$ in two ways.

The first way is to use the persistent cohomology of the initial data X to construct circular coordinates $X \rightarrow S^1$ and then embed the circle S^1 as the unit circle in the plane spanned by the first two coordinates of \mathbb{R}^D , $D \geq 2$, which gives us the initial map $\mathcal{X} \rightarrow \mathbb{R}^D$. In order to choose the

embedding dimension D , we compute the Stiefel–Whitney obstructions, as in Section 3.3. Since the base space is the circle, which is 1-dimensional, only the first Stiefel–Whitney class provides an obstruction. The Stiefel–Whitney class of the normal bundle of the embedding $S^1 \subseteq \mathbb{R}^D$ is trivial. Thus, if the first Stiefel–Whitney class of the estimated cocycle Ω is trivial, we set $D = r + 1$, and if it is non-trivial, we set $D = r + 2$.

The second way is to use the cut-unfold technique, explained next, with the circular coordinates and map $\mathcal{X} \rightarrow \mathbb{R}^D$ by embedding the interval $[0, 1)$ as the unit interval of the line spanned by the first coordinate of \mathbb{R}^D . In this case, since the interval is topologically trivial (contractible), the Stiefel–Whitney classes give no obstructions, and thus we set $D = r + 1$.

Cut-unfold technique. Some topologically non-trivial spaces can be described as a simple quotient of a simple topological space. For example, the circle S^1 is the quotient of the interval $[0, 1]$ that identifies 0 and 1. Thus, given a continuous map $\mathcal{X} \rightarrow S^1$, one gets a function $\mathcal{X} \rightarrow [0, 1)$, which is still continuous if we “cut” the topology of \mathcal{X} at the preimage of 0.

5 Examples

We apply FIBERED to three examples. We reproduce a dynamical system simulation from [13] and reconstruct one of its attractors—a torus. We reconstruct the conformation space—a Möbius band—and energy landscape of the pentane molecule from a simulation using RDKit [40]; this is inspired by an analysis in [30]. Finally, we reconstruct the conformation space of the cyclooctane molecule—a Klein bottle glued to a 2-sphere—using the data of [28].

We compare FIBERED to various well known dimensionality reduction algorithms (see Appendix B.4 for more plots). Table 1 summarizes the minimal target dimensions for which the algorithms are able to recover the topology of the data without tears or self intersections. Given that we consider topologically non-trivial data, we follow [41, 34] and evaluate the output of algorithms using persistent homology and persistence diagrams (PDs) to quantify the preservation of large scale topology (see Section 2 for background and references). When we do not clarify the field of coefficients used to compute a PD, the PD is independent of this choice.

For the initial map $\pi : X \rightarrow B$ we use the implementation of circular coordinates in [54]. The parameters for FIBERED are chosen as in Section 4.7. For persistent homology computations, we use Ripser [5] on geodesic distance, estimated as shortest path distance in a 15-nearest neighbor graph. For other dimensionality reduction algorithms, we use their Scikit-learn implementation [35].

	Optimal	Isomap	t-SNE	LE/DM	LLE	HLLE	LTSA	UMAP	FibeRed
Cylinder	2	3	3	3	3	3	3	3	2
Torus	3	4	4	4	4	4	4	4	3
Möbius band	3	4	4	3	N/A	N/A	N/A	3	3
Klein bottle	4	5	5	7	7	5	5	4	4

Table 1: The minimal target dimension that can be chosen for each of the algorithms considered in this section, so that there exist parameters that return a topologically faithful embedding of the data. “Optimal” refers to the theoretical minimal embedding dimension. “Cylinder” refers to the dataset of Fig. 1. “Torus”, “Möbius band”, and “Klein bottle” refer to the three datasets considered in this section. Since the Möbius band data is not Euclidean, some algorithms cannot be run on these data; we denote this with “N/A”.

Torus from attractor of double-gyre dynamical system. Dynamical systems can be analyzed by studying the topology of their attractors [2, 37]. Given a real-valued time series coming from measurements of a given particle on which a dynamical system acts, one can obtain a pointcloud by constructing a delay embedding of the time series, which, under certain conditions, is concentrated around a diffeomorphic copy of the attractor the particle is converging to [37]. Using the delay embedding method with target dimension 4, it was shown in [13, Section 4.1] that a certain attractor of the double-gyre dynamical system [47] is orientable, and has the homology of a torus. Here, we reproduce the simulation of [13], and apply dimensionality reduction to this 4D pointcloud, with the goal of embedding the attractor and its dynamics in \mathbb{R}^3 .

In Fig. 2, we show the results of FIBERED and t-SNE. In order to highlight self-intersections in low-dimensional representations, we use the following function: given a dataset X and a representation

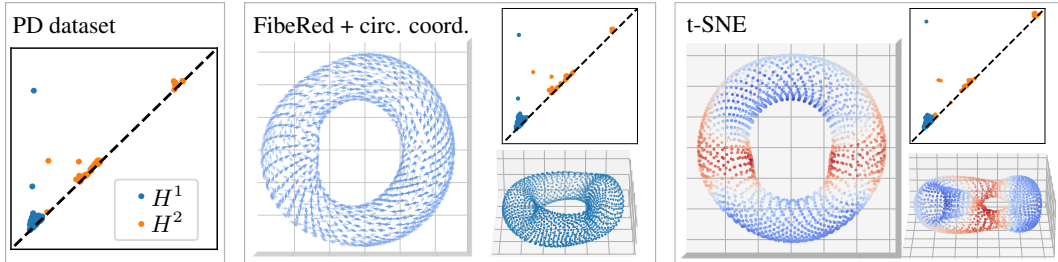


Figure 2: **1:** The PD of the original pointcloud (two prominent 1-dimensional classes, and one prominent 2-dimensional class). **2:** The output of FIBERED with the reconstructed dynamics and side view; and the PD of the output (which matches the PD of the original pointcloud well). **3:** The output of t-SNE on the same data and side view, colored by κ (red is smaller): there seem to be two self-intersections; and the PD of the output of t-SNE, which has one prominent 1-dimensional hole and two 2-dimensional voids, confirming that the red regions have been pinched.

of it $f : X \rightarrow Y$ let $\kappa : X \rightarrow \mathbb{R}$ be defined by $\kappa(x) = \min_{y \in X} d_Y(f(x), f(y)) / d_X(x, y)$. The output of t-SNE in Fig. 2 is representative of the output with other parameter choices and other dimensionality reduction algorithms we have tried on this data (LE, DM, LLE, HLLE, LTSA, Isomap, UMAP): if the target dimension is 3, there are always self-intersections or tears. The difficulty faced by metric-based algorithms in this example is that the input torus in 4D has a flat metric, and thus it does not admit a smooth isometric embedding in \mathbb{R}^3 .

Möbius band from conformation space of pentane. Any fixed molecule admits different realizations, or *conformations*, in three-dimensional space. In, e.g., molecular dynamics [19], one is interested in understanding all possible conformations of a molecule. The collection of conformations up to rotations and translations is known as the *conformation space* of the molecule. Each conformation has an associated energy, and the conformation space together with the energy function is known as the *energy landscape* of the molecule.

We reconstruct the conformation space and energy landscape of the pentane molecule from a simulation (see Appendix B.2 for details). The pentane molecule has two rotational degrees of freedom (modelled as a torus $S^1 \times S^1$), but also has a symmetry which interchanges the two angles of rotation. For this reason, the (unlabeled) conformation space consists of a quotient of the torus, which can be seen to be a Möbius band. In Fig. 3, we embed the conformation space of pentane in \mathbb{R}^3 , and compare the output of FIBERED to that of Isomap and t-SNE. LE and DM are able to recover a Möbius band in \mathbb{R}^3 ; since UMAP uses LE as initialization, it is also able to recover the Möbius band in \mathbb{R}^3 . In Fig. 4, we use the cut-unfold technique to find a fundamental domain of the conformation space, and estimate the energy landscape.

The difficulty faced by some of the metric-based dimensionality reduction algorithms in this example is that, with respect to the intrinsic metric, the ratio between the height of the Möbius band and its circumference is approximately $2/3$, and thus there is no isometric embedding in \mathbb{R}^3 [20, Theorem 15.1].

Klein bottle from conformation space of cyclooctane. In this example, we reconstruct the conformation space and energy landscape of the cyclooctane molecule using the dataset of [28]. In [28], it is shown that the conformation space of cyclooctane consists of a 2-sphere glued to a Klein bottle along two disjoint circles, and a parametrization of the dataset is given using Isomap and knowledge about how the data was generated.

In Fig. 5, we embed the Klein bottle part of the data in 4D. We were not able to recover the right topology in \mathbb{R}^4 using any of LE, DM, LLE, HLLE, LTSA, Isomap, or t-SNE. Meanwhile, UMAP is able to recover the right topology in \mathbb{R}^4 . In order to evaluate the 4D embeddings, we use the following distinguishing feature of the Klein bottle K : with $\mathbb{Z}/2$ coefficients we have $\dim(H^1(K; \mathbb{Z}/2)) = 2$ and $\dim(H^2(K; \mathbb{Z}/2)) = 1$, while with $\mathbb{Z}/3$ coefficients we have $\dim(H^1(K; \mathbb{Z}/3)) = 1$ and $\dim(H^2(K; \mathbb{Z}/3)) = 0$. In Fig. 6, we produce an efficient 2D parametrization of the conformation space of cyclooctane without using a priori knowledge of how the data was generated.

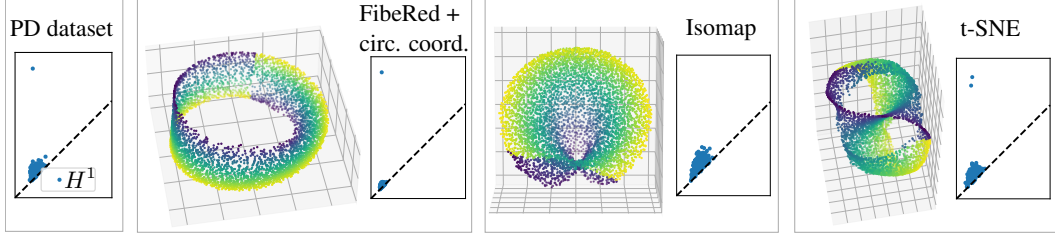


Figure 3: **1:** The PD of the original pointcloud, which has one prominent 1-dimensional class. **2:** The output of FIBEDED and its PD. **3:** The output of Isomap and its PD. Regardless of the parameter for Isomap, the algorithm is unable to capture the circularity of the data, and thus its PD has no prominent features. **4:** The output of t-SNE and its PD. Regardless of the parameters for t-SNE, the algorithm is unable to capture the circularity and non-orientability of the data without tears, which cause the output to have two holes. Outputs are colored by the fiber coordinate estimated by FIBEDED.

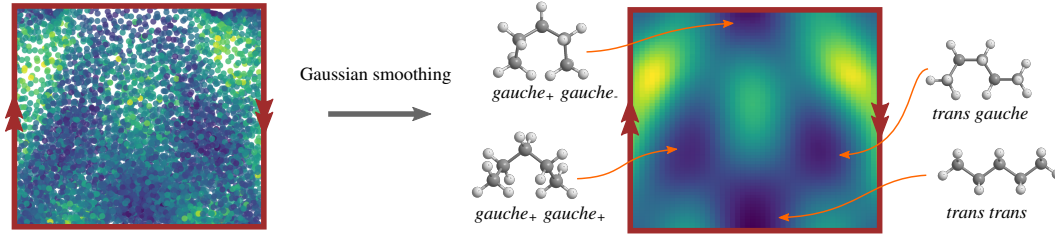


Figure 4: **Left:** the 2D representation of the conformation space of pentane using FIBEDED with the cut-unfold technique, colored by energy. Arrows indicate how the data must be glued in order to recover its global topology; this information can be extracted from the cocycle Ω of ESTCOCYCLES. **Right:** a 2D representation of the energy landscape of pentane, where the energy is estimated using the representation on the left and Gaussian smoothing. We see that there are four local minima of the energy function. By going back to the molecule simulation, we confirm that these four minima correspond to the four well known conformations of pentane [3].

The difficulty faced by metric-based algorithms in this example is that the Klein bottle in high dimensional space has aspect ratio close to 1 (i.e., an isometric representation by a fundamental domain such as the one of Fig. 6.2 has commensurable height and width), and thus it does not admit an isometric embedding in \mathbb{R}^4 .

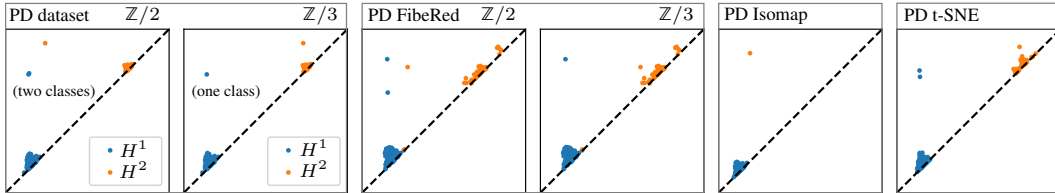


Figure 5: **1:** The PD of the original data with $\mathbb{Z}/2$ (two prominent 1-dimensional and one 2-dimensional classes) and $\mathbb{Z}/3$ coefficients (one prominent 1-dimensional class), which suggests the data is a Klein bottle. **2:** The PD of the 4D representation obtained using FIBEDED, which matches the original topology well. **3:** The PD of a 4D representation using Isomap. **5:** The PD of a 4D representation using t-SNE. For Isomap and t-SNE, the PD is the same regardless of the field of coefficients.

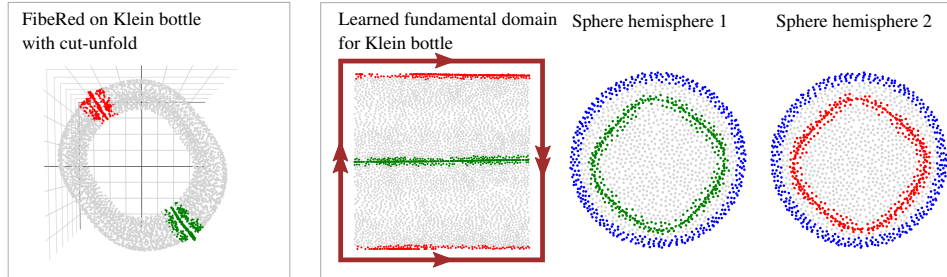


Figure 6: **1:** The output of FIBERED with the cut-unfold technique on the portion of the conformation space belonging to the Klein bottle. Colored in red and green are the two circles that glue the Klein bottle to the 2-sphere. Using this representation—a cylinder—we compute a new circular coordinate, which we combine with the initial circular coordinate to get a fundamental domain for the Klein bottle. **2:** A 2D model of the conformation space of cyclooctane. The two circles are two hemispheres of the 2D sphere, and were obtained using Isomap. Points not colored in grey indicate the gluings that have to be performed to recover the conformation space.

6 Discussion

We have presented a procedure to learn vector bundles from data, and demonstrated that it can be used to decouple the global topology from the local geometry in topologically complex data. We showed with examples that this can be helpful for embedding topologically complex data in low dimension, as well as for charting such data. We have also developed a sound mathematical foundation for this point of view.

Limitations. The theory and methods presented in this paper assume that the data lives in the total space of a vector bundle. There are two main ways in which real data can deviate from these assumptions: (1) There are singularities in the data manifold, and thus the base map is not a vector bundle since fibers may have different dimensions; (2) the data contains outliers, and only a core subset of the data satisfies the assumptions. Another important caveat is that (3) the procedure assumes that a base map is given. We comment on these remarks below.

Future work. With respect to (1), the situation in which the fibers of the base map can have different dimensions can be abstracted using the theory of stratified vector bundles [7, 6]. We believe that the main algorithm of Section 4 can be adjusted to account for different local dimensions by allowing the cocycle Ω between patches with different dimension to be a matrix in a Stiefel manifold, instead of an orthogonal matrix. With respect to (2), our procedures are robust with respect to limited amount of noise, and the problem of devising extensions robust to outliers is left as future work.

With respect to (3), there are several ways to obtain non-linear initial representations. First, other cohomological coordinates besides circular coordinates have been developed [36, 39]. Second, one could use standard non-linear representations, such as the ones learned by Diffusion Maps [24, 14]. Third, one could use any of the lens functions [50, Section 4] Mapper uses. Another interesting avenue for constructing coarse topological representations is to build a graph on the data, simplify it while preserving part of its large scale topology, and use a graph layout algorithm.

Finally, FIBERED can be interpreted as principal component analysis relative to an initial representation, as it works by linearly embedding the local coordinates of X that are not already accounted by the initial map, in a way that is globally consistent and orthogonal to the coordinates already accounted by the initial map. This suggests considering versions of other popular dimensionality reduction algorithms relative to an initial representation.

Acknowledgements. The authors thank Matt Piekenbrock for various fruitful conversations about dimensionality reduction. This work was partially supported by the National Science Foundation through grants CCF-2006661 and CAREER award DMS-1943758.

References

- [1] E. Aamari, J. Kim, F. Chazal, B. Michel, A. Rinaldo, and L. Wasserman. Estimating the reach of a manifold. *Electronic journal of statistics*, 13(1):1359–1399, 2019.
- [2] H. D. I. Abarbanel. *Analysis of observed chaotic data*. Institute for Nonlinear Science. Springer-Verlag, New York, 1996.
- [3] R. M. Balabin. Enthalpy difference between conformations of normal alkanes: Raman spectroscopy study of n-pentane and n-butane. *The Journal of Physical Chemistry A*, 113(6):1012–1019, 2009.
- [4] A. S. Bandeira, A. Singer, and D. A. Spielman. A Cheeger inequality for the graph connection Laplacian. *SIAM J. Matrix Anal. Appl.*, 34(4):1611–1630, 2013.
- [5] U. Bauer. Ripser: efficient computation of vietoris-rips persistence barcodes. *Journal of Applied and Computational Topology*, 2021.
- [6] H.-J. Baues and D. L. Ferrario. K -theory of stratified vector bundles. *K-Theory*, 28(3):259–284, 2003.
- [7] H.-J. Baues and D. L. Ferrario. Stratified fibre bundles. *Forum Math.*, 16(6):865–902, 2004.
- [8] M. Belkin and P. Niyogi. Laplacian eigenmaps for dimensionality reduction and data representation. *Neural computation*, 15(6):1373–1396, 2003.
- [9] I. Borg and P. J. F. Groenen. *Modern multidimensional scaling*. Springer Series in Statistics. Springer, New York, second edition, 2005. Theory and applications.
- [10] M. Brand. Charting a manifold. In S. Becker, S. Thrun, and K. Obermayer, editors, *Advances in Neural Information Processing Systems*, volume 15. MIT Press, 2002.
- [11] E. J. Cartan. Sur la possibilité de plonger un espace riemannien donné dans un espace euclidien. *Annales de la Société Polonaise de Mathématique*, 1928.
- [12] C. Casewit, K. Colwell, and A. Rappe. Application of a universal force field to organic molecules. *Journal of the American chemical society*, 114(25):10035–10046, 1992.
- [13] G. D. Charó, G. Artana, and D. Sciamarella. Topology of dynamical reconstructions from Lagrangian data. *Phys. D*, 405:132371, 12, 2020.
- [14] R. R. Coifman and S. Lafon. Diffusion maps. *Appl. Comput. Harmon. Anal.*, 21(1):5–30, 2006.
- [15] V. de Silva, D. Morozov, and M. Vejdemo-Johansson. Persistent cohomology and circular coordinates. *Discrete Comput. Geom.*, 45(4):737–759, 2011.
- [16] D. L. Donoho and C. Grimes. Hessian eigenmaps: Locally linear embedding techniques for high-dimensional data. *Proceedings of the National Academy of Sciences*, 100(10):5591–5596, 2003.
- [17] J. Garcia-Diaz, R. Menchaca-Mendez, R. Menchaca-Mendez, S. Pomares Hernández, J. C. Pérez-Sansalvador, and N. Lakouari. Approximation algorithms for the vertex k -center problem: Survey and experimental evaluation. *IEEE Access*, 7:109228–109245, 2019.
- [18] R. Ghrist. Barcodes: the persistent topology of data. *Bull. Amer. Math. Soc. (N.S.)*, 45(1):61–75, 2008.
- [19] J. M. Haile. *Molecular dynamics simulation: elementary methods*. John Wiley & Sons, Inc., 1992.
- [20] B. Halpern and C. Weaver. Inverting a cylinder through isometric immersions and isometric embeddings. *Trans. Amer. Math. Soc.*, 230:41–70, 1977.
- [21] A. Hatcher. *Algebraic topology*. Cambridge University Press, Cambridge, 2002.
- [22] R. A. Horn and C. R. Johnson. *Matrix analysis*. Cambridge University Press, Cambridge, second edition, 2013.
- [23] J. Jost. *Riemannian geometry and geometric analysis*. Universitext. Springer, Cham, seventh edition, 2017.
- [24] S. Lafon and A. Lee. Diffusion maps and coarse-graining: a unified framework for dimensionality reduction, graph partitioning, and data set parameterization. *IEEE Transactions on Pattern Analysis and Machine Intelligence*, 28(9):1393–1403, 2006.

- [25] J. A. Lee and M. Verleysen. Nonlinear dimensionality reduction of data manifolds with essential loops. *Neurocomput.*, 67:29–53, aug 2005.
- [26] A. V. Little, J. Lee, Y.-M. Jung, and M. Maggioni. Estimation of intrinsic dimensionality of samples from noisy low-dimensional manifolds in high dimensions with multiscale svd. In *2009 IEEE/SP 15th Workshop on Statistical Signal Processing*, pages 85–88. IEEE, 2009.
- [27] Z. Luo, C. Xu, Z. Zhang, and W. Jin. A topology-preserving dimensionality reduction method for single-cell rna-seq data using graph autoencoder. *Scientific reports*, 11(1):1–8, 2021.
- [28] S. Martin, A. Thompson, E. A. Coutias, and J.-P. Watson. Topology of cyclo-octane energy landscape. *The journal of chemical physics*, 132(23):234115, 2010.
- [29] L. McInnes, J. Healy, and J. Melville. Umap: Uniform manifold approximation and projection for dimension reduction, 2018.
- [30] I. Membrillo-Solis, M. Pirashvili, L. Steinberg, J. Brodzki, and J. G. Frey. Topology and geometry of molecular conformational spaces and energy landscapes, 2019.
- [31] J. W. Milnor and J. D. Stasheff. *Characteristic classes*. Annals of Mathematics Studies, No. 76. Princeton University Press, Princeton, N. J.; University of Tokyo Press, Tokyo, 1974.
- [32] M. Moor, M. Horn, B. Rieck, and K. Borgwardt. Topological autoencoders. In *International conference on machine learning*, pages 7045–7054. PMLR, 2020.
- [33] S. Y. Oudot. *Persistence theory: from quiver representations to data analysis*, volume 209 of *Mathematical Surveys and Monographs*. American Mathematical Society, Providence, RI, 2015.
- [34] R. Paul and S. K. Chalup. A study on validating non-linear dimensionality reduction using persistent homology. *Pattern Recognition Letters*, 100:160–166, 2017.
- [35] F. Pedregosa, G. Varoquaux, A. Gramfort, V. Michel, B. Thirion, O. Grisel, M. Blondel, P. Prettenhofer, R. Weiss, V. Dubourg, J. Vanderplas, A. Passos, D. Cournapeau, M. Brucher, M. Perrot, and E. Duchesnay. Scikit-learn: Machine learning in Python. *Journal of Machine Learning Research*, 12:2825–2830, 2011.
- [36] J. A. Perea. Multiscale projective coordinates via persistent cohomology of sparse filtrations. *Discrete Comput. Geom.*, 59(1):175–225, 2018.
- [37] J. A. Perea. Topological times series analysis. *Notices Amer. Math. Soc.*, 66(5):686–694, 2019.
- [38] J. A. Perea. Sparse circular coordinates via principal \mathbb{Z} -bundles. In *Topological data analysis—the Abel Symposium 2018*, volume 15 of *Abel Symp.*, pages 435–458. Springer, Cham, 2020.
- [39] L. Polanco and J. A. Perea. Coordinatizing data with lens spaces and persistent cohomology. In Z. Friggstad and J. D. Carufel, editors, *Proceedings of the 31st Canadian Conference on Computational Geometry, CCCG 2019, August 8-10, 2019, University of Alberta, Edmonton, Alberta, Canada*, pages 49–58, 2019.
- [40] RDKit developers. RDKit: Open-source cheminformatics. <http://www.rdkit.org>, 2022.
- [41] B. Rieck and H. Leitte. Persistent homology for the evaluation of dimensionality reduction schemes. In *Computer Graphics Forum*, volume 34, pages 431–440. Wiley Online Library, 2015.
- [42] S. Roweis, L. Saul, and G. E. Hinton. Global coordination of local linear models. In T. Dietterich, S. Becker, and Z. Ghahramani, editors, *Advances in Neural Information Processing Systems*, volume 14. MIT Press, 2001.
- [43] S. T. Roweis and L. K. Saul. Nonlinear dimensionality reduction by locally linear embedding. *science*, 290(5500):2323–2326, 2000.
- [44] A. Sadeghi, S. A. Ghasemi, B. Schaefer, S. Mohr, M. A. Lill, and S. Goedecker. Metrics for measuring distances in configuration spaces. *The Journal of chemical physics*, 139(18):184118, 2013.
- [45] L. Scoccola and J. A. Perea. Approximate and discrete Euclidean vector bundles, 2021.
- [46] L. Scoccola and J. A. Perea. FibeRed implementation. <https://github.com/LuisScoccola/fibered.git>, 2022.

- [47] S. C. Shadden, F. Lekien, and J. E. Marsden. Definition and properties of Lagrangian coherent structures from finite-time Lyapunov exponents in two-dimensional aperiodic flows. *Phys. D*, 212(3-4):271–304, 2005.
- [48] A. Singer. Angular synchronization by eigenvectors and semidefinite programming. *Appl. Comput. Harmon. Anal.*, 30(1):20–36, 2011.
- [49] A. Singer and H.-t. Wu. Orientability and diffusion maps. *Appl. Comput. Harmon. Anal.*, 31(1):44–58, 2011.
- [50] G. Singh, F. Mémoli, G. E. Carlsson, et al. Topological methods for the analysis of high dimensional data sets and 3d object recognition. *PBG Eurographics*, 2, 2007.
- [51] J. Tang, J. Liu, M. Zhang, and Q. Mei. Visualizing large-scale and high-dimensional data. In *Proceedings of the 25th International Conference on World Wide Web, WWW '16*, pages 287–297, Republic and Canton of Geneva, CHE, 2016. International World Wide Web Conferences Steering Committee.
- [52] Y. Teh and S. Roweis. Automatic alignment of local representations. In S. Becker, S. Thrun, and K. Obermayer, editors, *Advances in Neural Information Processing Systems*, volume 15. MIT Press, 2002.
- [53] J. B. Tenenbaum, V. d. Silva, and J. C. Langford. A global geometric framework for nonlinear dimensionality reduction. *Science*, 290(5500):2319–2323, 2000.
- [54] C. Tralie, T. Mease, and J. Perea. Dreimac. <https://github.com/ctralie/DREiMac>, 2017.
- [55] L. Van der Maaten and G. Hinton. Visualizing data using t-SNE. *Journal of machine learning research*, 9(11), 2008.
- [56] A. Wagner, E. Solomon, and P. Bendich. Improving metric dimensionality reduction with distributed topology, 2021.
- [57] H. Whitney. The self-intersections of a smooth n -manifold in $2n$ -space. *Ann. of Math. (2)*, 45:220–246, 1944.
- [58] L. Yan, Y. Zhao, P. Rosen, C. Scheidegger, and B. Wang. Homology-preserving dimensionality reduction via manifold landmarking and tearing. *arXiv preprint arXiv:1806.08460*, 2018.
- [59] Z. Zhang and H. Zha. Principal manifolds and nonlinear dimensionality reduction via tangent space alignment. *SIAM Journal on Scientific Computing*, pages 313–338, 2004.

A Proofs

Since we use this in both proofs, note that, by definition of the normal bundle $N \rightarrow \mathcal{B}$, Problem 1 admits a solution $j : N \rightarrow \mathbb{R}^D$ when $\mathcal{X} = N$. In particular, for each $b \in \mathcal{B}$, we have a bijection $j|_{\nu^{-1}(b)} : \nu^{-1}(b) \rightarrow j(\nu^{-1}(b))$.

Proof of Lemma 2. We start with the “if” direction. Given a morphism $\mathcal{X} \rightarrow N$ that is injective and an isometry in each fiber gives, by postcomposition with j , a fiberwise isometric embedding $\mathcal{X} \rightarrow \mathbb{R}^D$ satisfying the requirements in the statement of Problem 1.

For the other direction, assume given an isometric embedding $\bar{\iota} : \mathcal{X} \rightarrow \mathbb{R}^D$ satisfying the requirements in the statement of Problem 1. Since $\bar{\iota}$ extends ι and is orthogonal to \mathcal{B} , its image is contained in the image of $j : N \rightarrow \mathbb{R}^D$. The claim now follows from the fact that $\bar{\iota}$ and j are linear isometries in each fiber. \square

Proof of Proposition 3. We start with the “if” direction. Given the maps $\Phi = \{\Phi_i : U_i \rightarrow \mathbb{V}(d, D - e)\}$ as in the statement, one defines a map $\mathcal{X} \rightarrow N$ by

$$X_i \ni x \mapsto (j|_{\nu^{-1}(b)})^{-1}(\alpha_i(\pi(x))\Phi_i(\pi(x))f_i(x) + \iota(\pi(x))) \in N,$$

which, using Eq. (5), is easily seen to be a well-defined linear isometry in each fiber.

For the other direction, suppose given a morphism of vector bundles $g : \mathcal{X} \rightarrow N$ that is injective and a linear isometry in each fiber. Using the fact that g is linear, one sees that there exists a unique map $\Phi_i : U_i \rightarrow \mathbb{V}(d, D - e)$ satisfying

$$\Phi_i(\pi(x))^T \alpha_i(\pi(x))^T (j(g(x)) - \iota(\pi(x))) = f_i(x),$$

for all $x \in U_i$. This also implies, in particular, that the family of maps $\{\Phi_i\}$ satisfies Eq. (5). \square

B More about examples and implementation

B.1 Efficiency

We comment on the complexity of the main subroutines of FIBERED. Let $N = |X|$. The greedy approach to the k -center problem implemented by COVERANDPARTITIONUNITY has time complexity in $O(kN)$. LOCALLINEARREPRESENTATION and ESTTANGANDNORMBUN require $O(k)$ SVD computations, with matrices of size $|X_i|$ for each i , which at most N . There is room for improvement here, since only the d and D largest singular values are required, respectively, and $|X_i|$ can be made significantly smaller than N by making larger k . Another significant improvement would be to use landmark MDS instead of MDS for LOCALLINEARREPRESENTATION. ESTNORMFIBERCOORDINATES requires $O(k)$ least squares solutions to a linear system, which can be implemented using SVD with matrices of size e . ESTREACH requires $O(k^2)$ direct calculations. ESTCOCYCLES requires $O(k^2)$ SVD. Finally, ALIGNFIBERS requires $O(n_iter)$ SVD with matrices of size $D - e$.

B.2 Pentane data generation

We used RDKit’s function EmbedMolecule with different random initializations to get a sample of 20000 conformers of pentane. We set useExpTorsionAnglePrefs to False in order to obtain a good sample of the full conformation space, rather than just conformers with low energy. We then computed pairwise distances between all conformers using GetBestRMS, which computes the root-mean-square deviation (see, e.g., [44]). In order to speed up the computation of pairwise distances, we compare the conformers after removing the hydrogen atoms and keeping the carbon atoms. Finally, we kept a subsample of 5000 conformers that approximates the full sample well. The energy of conformers was calculated using universal force field [12].

B.3 Computation of Stiefel–Whitney obstructions

We describe how we compute Stiefel–Whitney classes associated to the vector bundles approximated by the cocycle Ω computed by ESTCOCYCLES in each of the three examples. For this we use the algorithms of [45, Theorem C] and follow the technique in [45, Section 7.1].

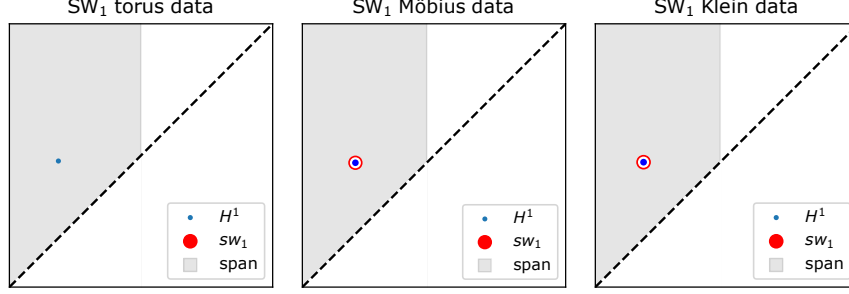


Figure 7: The persistence diagram of $\{\mathcal{N}_r\}_{r \in [0,1]}$ for each of the three examples, with the span of Ω shaded in grey, and the classes summing to $w_1(\Omega)$ circled in red. Recall that in the three examples, the nerve \mathcal{N} is a circle, and thus the persistence diagram consists of just one prominent 1-dimensional cohomology class. In the case of the torus, the first Stiefel–Whitney class is zero, and thus there is no obstruction to choosing $D = 1 + 2$ (1 being the dimension of the circle, and 2 the rank of the vector bundle). In the case of the Möbius band, the first Stiefel–Whitney class coincides with the only point in the persistence diagram, and is thus non-trivial, which gives an obstruction to selecting $D = 1 + 1$, which reflects the fact that the Möbius band cannot be embedded in the plane. Similarly, in the case of the Klein bottle, the Stiefel–Whitney computation gives an obstruction to selecting $D = 1 + 2$, which reflects the fact that the Klein bottle cannot be embedded in \mathbb{R}^3 .

By construction, Ω is a discrete approximate cocycle on the simplicial complex \mathcal{N} . Recall that an edge (ij) of \mathcal{N} is associated the weight $s_{ij} = |X_i \cap X_j|$. This determines a filtration of the simplicial complex \mathcal{N} , which we denote by $\{\mathcal{N}_r\}_{r \in [0,1]}$ where vertices are born at 0, edges at $1 - s_{ij}/|X|$, and higher simplices are born when all of their edges appear. In this way, \mathcal{N}_0 consists of just vertices and $\mathcal{N}_1 = \mathcal{N}$. As in [45, Section 7.1], we define the *death* of Ω as the supremum over all $r \in [0, 1]$ such that Ω is a 2-approximate cocycle on \mathcal{N}_r , and the *span* of Ω as the region of the persistence diagram of classes that are born before the death of Ω . This is the region of classes that can appear in the support of $w_1(\Omega)$.

In Fig. 7, we show the result of performing these computations in the three examples of Section 5 of the paper.

B.4 Other runs

We run Isomap, LLE, HLLE, LTSA, Laplacian Eigenmaps, Diffusion Maps, t-SNE, UMAP on the datasets of the paper. We vary the main parameter for each algorithm. We report here the results of the cylinder (Fig. 8), torus (Fig. 9), and Klein bottle data (Fig. 10), as these can be judged by looking 2D plots. For t-SNE we use the PCA initialization, except for the Möbius band data, which is not Euclidean.

As in the paper, we report persistent homology of a Vietoris–Rips complex on geodesic distance, computed as shortest path distance on a 15-nearest neighbor graph.

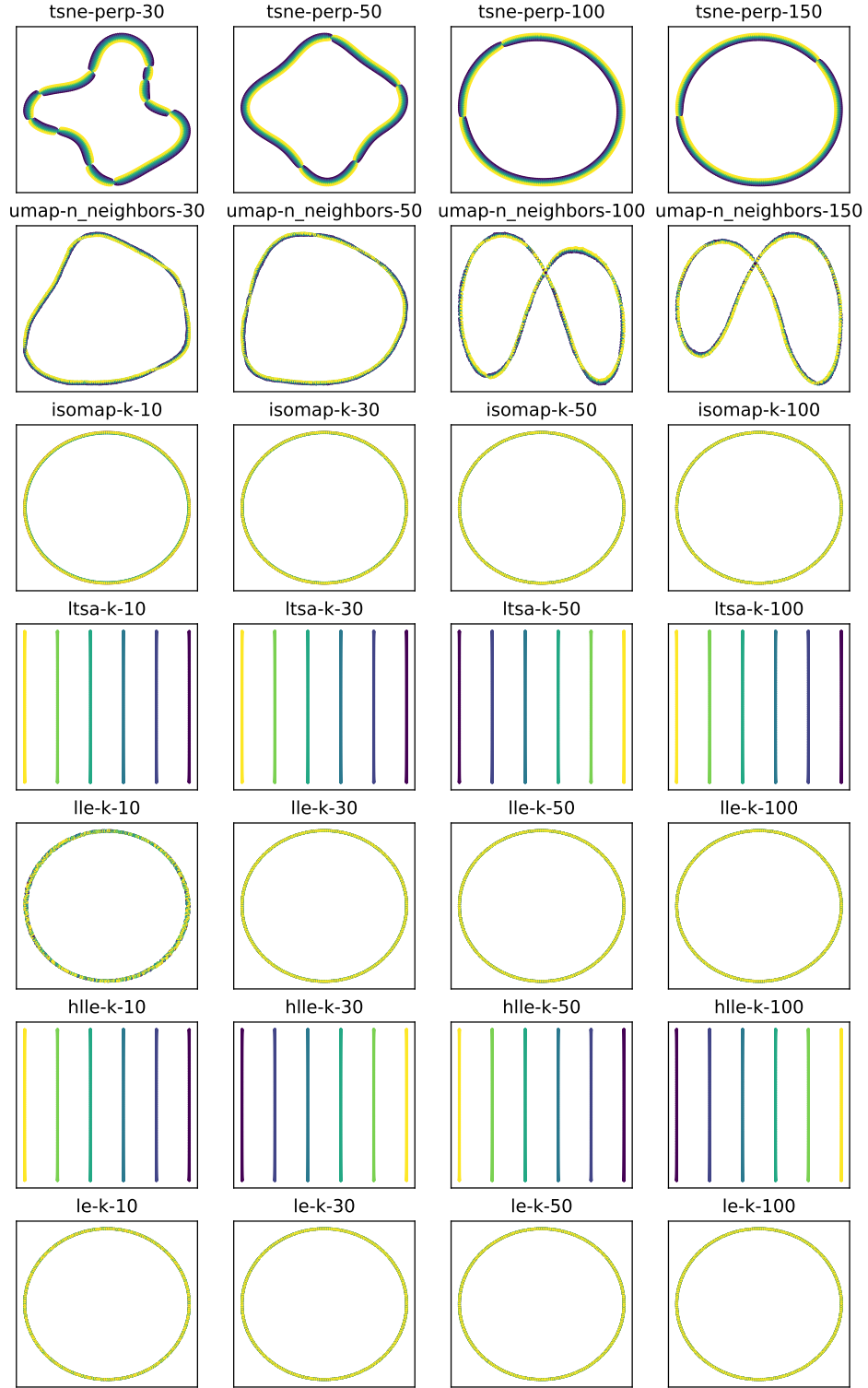


Figure 8: We see that no output is able to consistently align the local 2D structure around the circularity of the cylinder. We do not include the results of running Diffusion Maps (the results are not significantly different from those of Laplacian Eigenmaps).

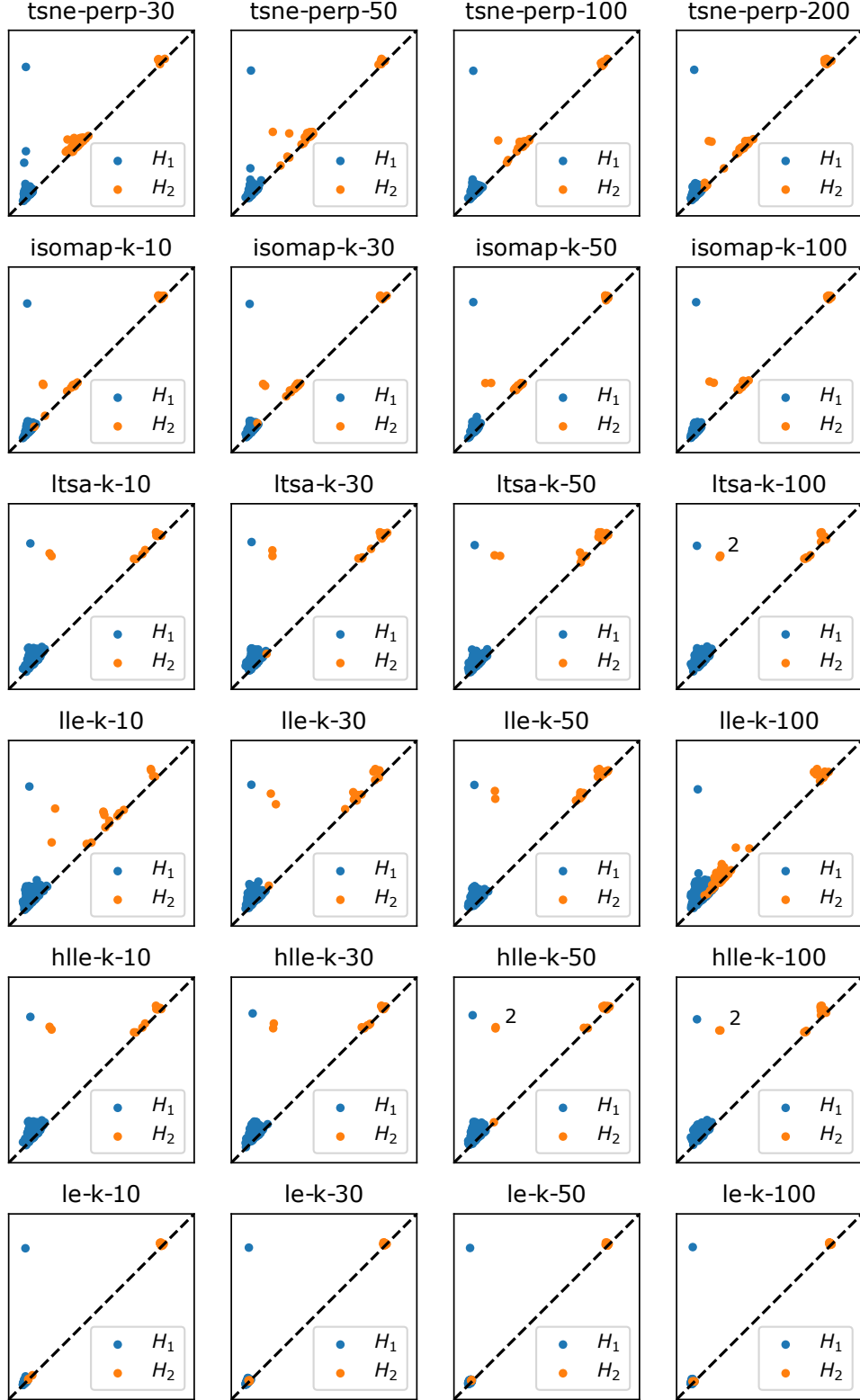


Figure 9: Recall that the torus T has homology $\dim(H_1(T; \mathbb{Z}/2)) = 2$ and $\dim(H_2(T; \mathbb{Z}/2)) = 1$. We see that no output has two prominent 1-dimensional classes and one prominent 2-dimensional class. Persistent homology was computed with $\mathbb{Z}/2$ coefficients. When there are two classes that almost overlap, we mark them with a 2. We do not include the results of running Diffusion Maps (the results are not significantly different from those of Laplacian Eigenmaps) and UMAP (the results are not significantly different from those of t-SNE).

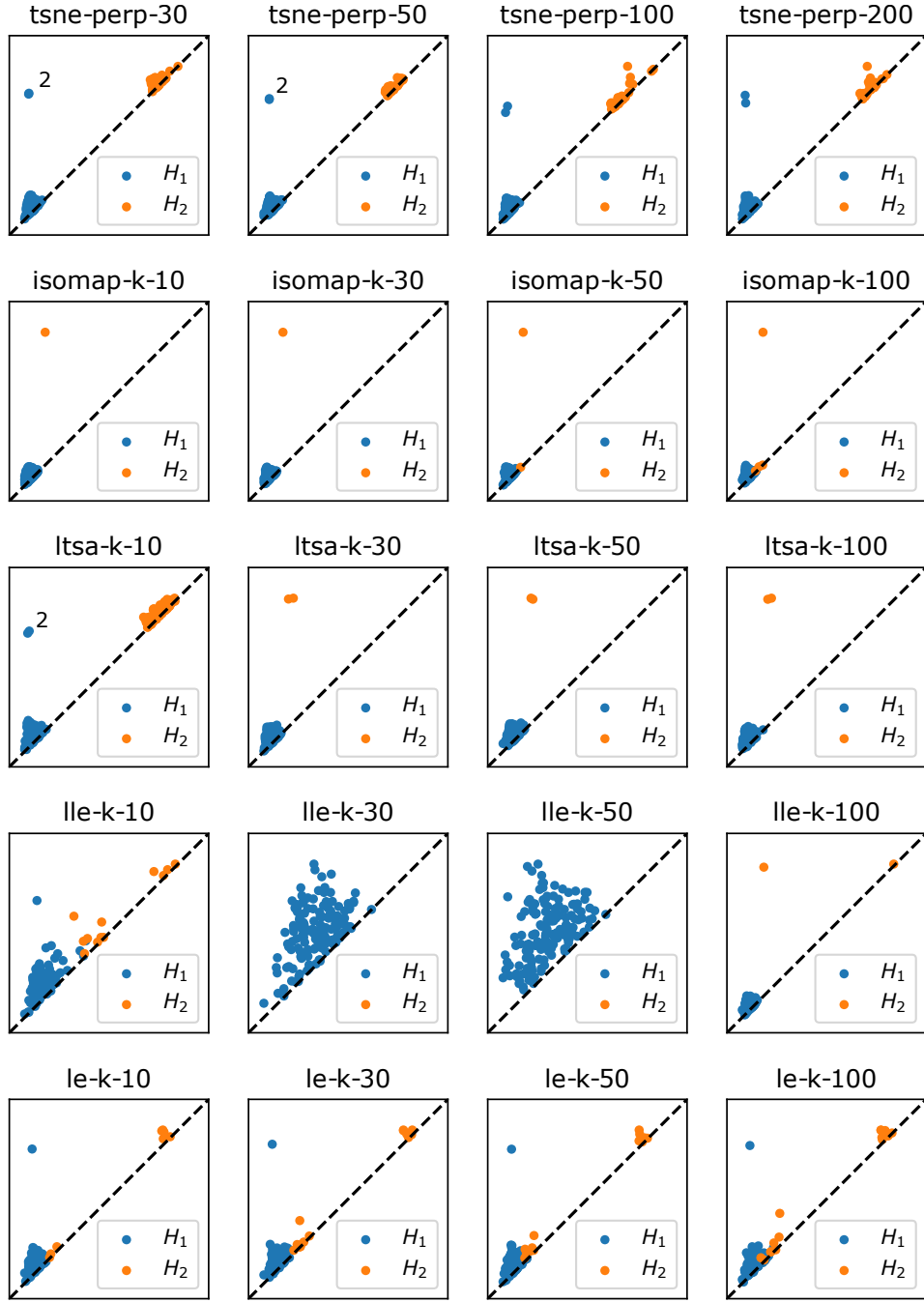


Figure 10: Recall that, if K is the Klein bottle, with $\mathbb{Z}/2$ coefficients we have $\dim(H_1(K; \mathbb{Z}/2)) = 2$ and $\dim(H_2(K; \mathbb{Z}/2)) = 1$, while with $\mathbb{Z}/3$ coefficients we have $\dim(H_1(K; \mathbb{Z}/3)) = 1$ and $\dim(H_2(K; \mathbb{Z}/3)) = 0$. We are displaying persistent homology with $\mathbb{Z}/2$ coefficients, which, for all the examples, coincides with the persistence homology with $\mathbb{Z}/3$ coefficients. We see that no output exhibits the homology of the Klein bottle. When there are two classes that almost overlap, we mark them with a 2. In this example, HLE runs fails when computing eigenvectors, since the data manifolds is not developable. We do not include the results of running Diffusion Maps (the results are not significantly different from those of Laplacian Eigenmaps).